


Research Article

Deformation and Failure Evolution Law and Support Optimization of Gob-Side Entry in Weakly Cemented Soft Rock under the Influence of Fault

Chengfu Ma,^{1,2} Fenghai Yu ,^{1,3} Kai Zhou ,^{1,3} Xuerui Yang,^{1,3} Bo Sun,^{1,3} Xinyu Yao,² Yan Chi,⁴ and Yuanzhi Zhang²

¹College of Energy and Mining Engineering, Shandong University of Science and Technology, Qingdao 266590, China

²Ordos Haohua Hongqingliang Mining Co., Ltd., Ordos 014300, China

³State Key Laboratory of Mining Disaster Prevention and Control, Shandong University of Science and Technology, Qingdao 266590, China

⁴Qingdao Shunqingyuan Environment Co., Ltd., Qingdao 266590, China

Correspondence should be addressed to Fenghai Yu; sdustfh@163.com

Received 5 January 2023; Revised 21 March 2024; Accepted 20 April 2024; Published 16 May 2024

Academic Editor: Vasudevan Rajamohan

Copyright © 2024 Chengfu Ma et al. This is an open access article distributed under the Creative Commons Attribution License, which permits unrestricted use, distribution, and reproduction in any medium, provided the original work is properly cited.

Under the condition of weakly cemented soft rock in Western China, the surrounding rock deformation of gob-side entry is obvious, especially under the influence of fault, and the problem of surrounding rock control becomes increasingly prominent. To solve this issue, this paper firstly studied and obtained the evolution law of the ground pressure appearance of the gob-side entry in the fault area, then put forward the concept of surrounding rock control in the fault area of the gob-side entry, put forward a targeted pressure relief + increase preload + passive reinforcement parallel to the roadway surrounding rock strengthening control scheme, and carried out field applications. The results show that the roof subsidence and mining side heave of the roadway in the fault area increase significantly, accompanied by the characteristics of broken cables, the length of the broken cable is 0.2 m–0.6 m, and the breaking process is divided into multiple breaks. The stress evolution of gob-side entry in fault area presents a stage characteristic of “rapid growth-stable.” The surrounding rock control effect is improved under the bolt cable high pretightening support, and the roadway deformation is effectively controlled under the pressure relief + active + passive support, with a good application effect.

1. Introduction

China’s western Inner Mongolia region is rich in coal resources and has become the main mining and production force [1]. However, weakly cemented soft rocks are widely distributed in the western Inner Mongolia region. Such soft rocks have low strength and poor cementation and are prone to argillization when meeting water, which seriously affects the stability of the gob-side roadway. Especially when the roadway is affected by faults, the gob-side roadway is prone to significant deformation, support failure, and other phenomena [2, 3].

At present, many experts and scholars have carried out a series of studies on the stability of roadways in fault areas and obtained many key research results. In terms of roadway deformation affected by faults, Shan [4, 5] proposed that the roadway presents asymmetric deformation under the influence of faults and mining, obtained the influence mechanism of different faults on roadway deformation and damage, and proposed that the roadway damage in the area affected by the fault layer during the mining process presents a secondary increase trend. Many scholars have studied the deformation and failure mechanism of roadways in fault areas. Liu [6] proposed that the low strength and softening of

surrounding rock is the internal cause of surrounding rock deformation, and the high crustal stress is the external cause. Sun [7] proposed that the superposition effect of advance support pressure, lateral support pressure, and fault structure has a great impact on the distribution of the maximum principal stress of roadway surrounding rock. Ma [8] found that the fault slip and relocation caused by coal mining would cause rock strata to be affected and broken.

In terms of fault area support, Wang [9] proposed a new support design for cable, and Xie [10] proposed an integrated control technology of bolting and grounding. At the same time, active and passive combined support has also been widely used, such as double layer truss technology [11], grounding+cable anchor [12], and closed support+grounding+mesh cable [13]. The above support techniques can effectively control the stability of the roadway in fault areas.

However, at present, the research on support control in fault areas under weakly cemented soft rock conditions still needs to be strengthened, especially since the field measurement of rock pressure evolution mechanism in fault areas is less. In this paper, through the combination of field measurement and numerical simulation, through obtaining the evolution law of roadway failure and instability in the weakly cemented soft rock under fault conditions, the optimization technology of roadway support is proposed and applied in the field.

2. Site Descriptions and Monitoring Scheme

11302 working face is the second mining face of the 3-1 coal seam of the mine, with a buried depth of about 450 m–500 m and a coal seam thickness of about 4.1 m–6.0 m. The 11302 tail entry is a gob-side roadway. The driving process is to first drive the 11302 belt roadway, then drive the waist roadway in the middle of the working face, and finally drive from the waist roadway to the cut hole and the main roadway to form the 11302 tail entry. There is a J10 normal fault at the intersection of the roadway and the waist roadway, with a maximum fault distance of 2.7 m. The specific roadway engineering and geological conditions are shown in Figure 1.

HB24 # geological borehole is close to the fault location. According to the HB24 # borehole, the roof of this area is mainly composed of sandy mudstone and conglomerate, of which the sandy mudstone is 19.8 m thick.

The top and bottom floors of 11302 working face are mainly composed of sandy mudstone and conglomerate. The coal seams and top sandy mudstone of the working face were sampled and tested, and the average uniaxial compressive strength of coal and sandy mudstone was 21.63 MPa and 17.45 MPa, respectively. The main mineral components of sandy mudstone are quartz, chlorite, muscovite, etc. Among them, chlorite is the main clay mineral with a high total content. It is easy to mud in water and has low strength. Therefore, the surrounding rock of the top and bottom of the 11302 working face belongs to weakly cemented soft rock. The conglomerate layer is relatively high, and the strength cannot be determined due to the difficulty in sampling. However, the characteristics such as the difficulty in drilling

and the lack of internal stratification during the drilling process indicate that the conglomerate strength is relatively high. The specific lithology and thickness of the roof and floor are shown in Table 1.

Due to the stress concentration in the fault area, it is easy to produce significant ground pressure, so the weakly cemented soft rock gob-side entry affected by the fault and the area not affected by the fault are monitored separately, which are divided into three monitoring areas, of which 1 # and 3 # monitoring areas are not affected by the fault, and 2 # monitoring area is affected by J10 normal fault. On site mining pressure monitoring methods. Mainly including roadway surface displacement, borehole TV, and borehole stress, respectively, explored the deformation and failure evolution law of 11302 tail entry in tunneling and mining periods. Two survey points are arranged in each survey area, and each survey point is subjected to the above two monitoring methods with a spacing of 10–15 m. The specific monitoring scheme is shown in Figure 2.

3. Evolution Law of Deformation and Failure of Gob-Side Entry under the Influence of Fault

3.1. Characteristics of Macroscopic Rock Pressure Manifestation. The 11302 tail entry has obvious jacking in the 2 # monitoring area (affected by the fault). The shoulder of the roadway has severely bulged. The metal steel belt and channel steel in the severe part have severe deformation, and the cable has a serious failure. The 1 # and 3 # monitoring areas (not affected by the fault) have slight roof subsidence and floor heave, and there is no failure of bolts, cables, and other supports. The overall integrity of the roadway is good, as shown in Table 2. From the macroscopic rock pressure appearance degree, the fault has a significant impact on the weakly cemented soft rock gob-side entry, showing a significant roadway deformation phenomenon.

At the same time, the gob-side tunnel has obvious failure phenomena such as cables in the fault area. According to the breaking situation of cables on-site, most of the cables are broken in strands, and the breaking time of each strand is inconsistent. As shown in Figure 3, the length of the broken cable is 0.2 m–0.6 m (regardless of the exposed end), and the fracture is uneven. According to the corrosion degree of the fracture surface, the breaking sequence of each strand can be judged. Most of the seven strands of cable are broken 2-3 times.

There are mainly two types of cable breaking failure: the central steel strand is broken first and the central steel strand is broken last, as shown in Table 3. Most of the cables are broken, the outer ring steel strand stubs are severely rusted, and the central steel strand stubs are relatively new. Among them, the number of cables broken in three times is the largest, most of which are 3 cables broken in the first time, 3 cables broken in the second time, and 1 cable broken in the third time.

The failure characteristics of the cable are mainly brittle fracture at the fracture of each steel strand, and the diameter shrinkage is not obvious. The failure of the cable in the fault area is characterized by dynamic load fracture. As

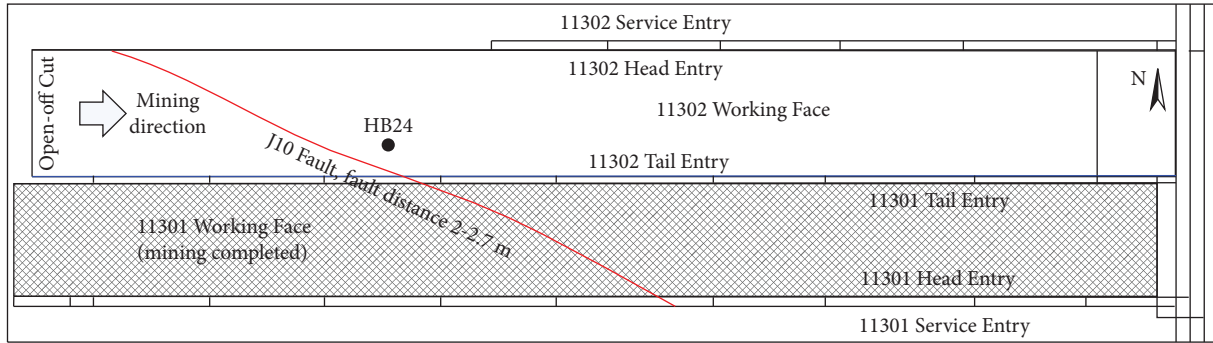


FIGURE 1: Engineering geology of 11302 working face.

TABLE 1: Distribution of rock layers on the roof and floor of working face 11302.

Lithology	Thickness (m)	Description
Conglomerate	15.08	Light gray, grayish white, containing rock debris and mica fragments, filled with mud
Sandy mudstone	19.78	Gray siltstone and dark gray sandy mudstone, locally containing plant fossils, parallel bedding development
Coal	4.26	Black block shaped, mainly composed of dark coal, followed by bright coal, with weak asphalt luster and strip-shaped structure
Sandy mudstone	20.01	Gray siltstone and dark gray sandy mudstone, containing plant fossils locally, and developing parallel bedding

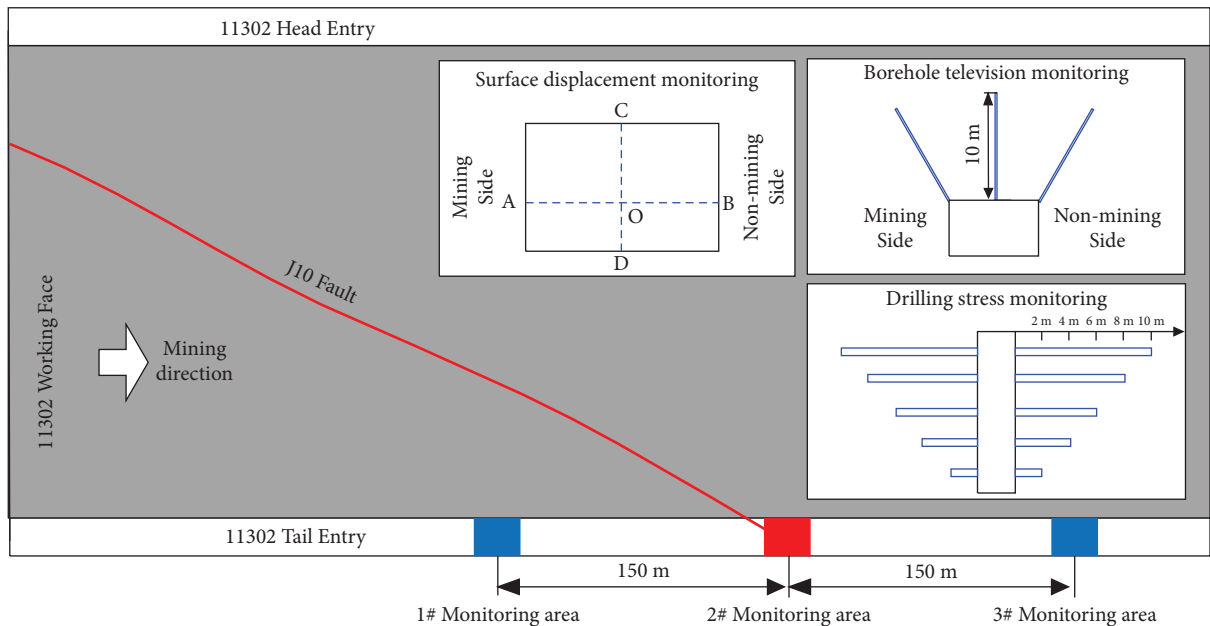


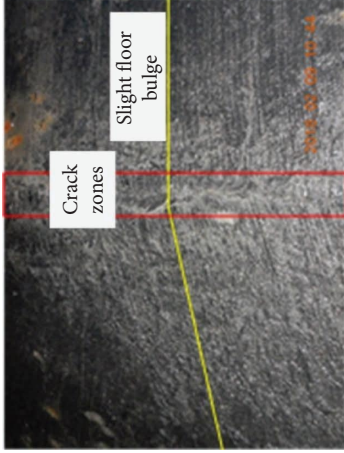
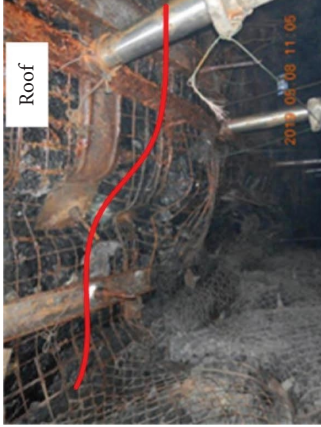

FIGURE 2: Roadway monitoring area and monitoring scheme.

can be seen from Figure 4, the gob-side roadway in the fault area receives a high static load, and the cable is in a tension state. At this time, the dynamic load disturbance transmitted with mining and other roof activities is easy to break when the individual steel strand reaches the tension deformation limit, and the tensile capacity of the cable decreases. Other steel strands break under high static load, resulting in obviously broken characteristics. However, the form of steel strand breakage at the center of the cable is different, which is mainly related to factors such as the

installation angle of the cable. When the cable is perpendicular to the coal wall, it is easy for the steel strand at the center position to break.

3.2. Analysis of Specific Monitoring Results. Continuous ground pressure monitoring was carried out for 1 #, 2 #, and 3 # survey areas, including surface displacement, borehole peeping, and borehole stress, to obtain the overall ground pressure evolution law of the goaf roadway affected by faults.

TABLE 2: Characteristics of ground pressure behavior in different monitoring areas.

Monitoring area	Macroscopic strata behavior	Main deformation characteristics
1#	Slight roof subsidence occurs in the roadway, the floor heave is not obvious, and the wall bulge is not found	 <p>The photograph shows a close-up of a roadway floor. A red dashed line indicates 'Crack zones' across the width. A yellow line indicates a 'Slight floor bulge' in the center. A timestamp '2015-03-09 11:44' is visible in the bottom right corner.</p>
2#	The roadway roof sinks significantly, with floor heave to a certain extent, and the mining side heaves more than the coal pillar wall	 <p>The photograph shows a roadway roof with a red line tracing a significant downward curve, labeled 'Roof'. A timestamp '2015-03-09 11:05' is visible in the bottom right corner.</p>
3#	Regional roof subsidence occurs in the roadway, the roadway roof is poorly formed, the floor heave is slight, and no obvious wall heave occurs	 <p>The photograph shows a roadway with a red line tracing a curve in the roof, labeled 'Roof sinking'. A timestamp '2015-10-03 13:29' is visible in the bottom right corner.</p>

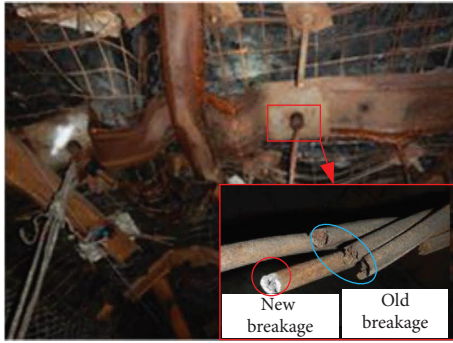


FIGURE 3: Photo of partial strand breaking cable in the fault area.

3.2.1. Surface Displacement Monitoring. The change of roadway surface displacement in the three monitoring areas is shown in Figure 5.

The overall roadway at 1 # and 3 # measuring points along with the mining face remains basically stable. The roadway mainly shows a trend that the roof displacement is greater than the floor, and the mining side and non-mining side bulges are similar. The roof and floor displacement are relatively large; the 2 # measuring point is located in the fault area. Until the end of the monitoring, the roof subsidence of the roadway has increased by 294% and 232%, respectively, compared with 1 # and 3 # measuring points. The roof subsidence is significant. At the same time, the mining wall shows obvious bulge. At 35 m from the working face, it has increased by 500 mm compared with 48 m, showing a sudden increase trend. The wall bulge is fast and large.

3.2.2. Borehole Television Detection. The roof of three different monitoring areas was peeped through boreholes, and the specific detection results are shown in Figure 4. In the three monitoring areas, there are obvious fractures in the top coal area and a large degree of separation between the top coal and roof mudstone. The roof damage range of the area not affected by the fault (1 # survey area and 3 # survey area) is within the depth range of 0–3 m, and the overall roadway roof fragmentation and damage range are small. In the area affected by the fault (2 # survey area), the main roof separation fracture area is mainly distributed within the range of 0–5 m drilling depth. The specific fracture locations are 0–1 m (located in the top coal), 1.1 m~1.2 m (located at the coal rock boundary), 1.4 m, 1.8 m, 2.5 m, 3.5 m, and 5 m. Among them, the separation layer at the coal rock interface is cracked most seriously, and the scope and extent of roof damage have increased significantly. At this time, the roof at the free section of the cable has a large area of separation layer subsidence, leading to a significant reduction in the integrity of the roadway, and the cable is seriously ineffective under the effect of high stress and large deformation.

3.2.3. Drilling Stress Monitoring. Representative borehole stress data are selected at the locations of 1 #, 2 #, and 3 # measuring points, and the stress distribution near the roadway is shown in Figure 6.

The distribution trend of borehole stress in the fault area is quite different from that in the area not affected by the fault: the borehole stress in the 2 # survey area shows a sharp increase trend within 50 m behind the driving face, and the borehole stress outside 50 m behind the working face is gradually stable, with the maximum vertical stress reaching about 9.9 MPa. The drilling stresses in 1 # and 3 # survey areas are about 35 m and 30 m behind the working face, respectively, and tend to be stable, indicating that under the combined influence of fault and tunneling, the stability time of the roadway increases, the vertical stress increment is significant, and the overall pressure of the roadway in the fault area is large.

3.3. Stress Evolution Law of Gob-Side Entry. The stress in the normal area and the area affected by the fault after tunneling along the goaf presents a stress change trend of “surge stage-stable stage.” The stress in the normal area tends to be stable after 30–35 m of tunneling, and the loose range of the surrounding rock of the roadway is basically less than 3 m. At this time, the cable can play a better supporting role, and the overall deformation of the roadway is controllable.

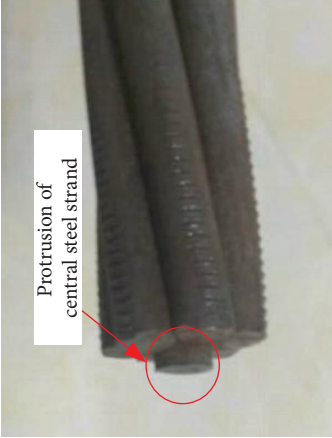
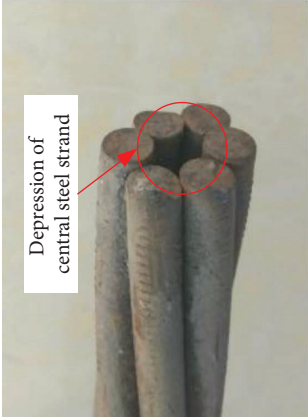
In the roadway in the fault-affected area, the stress of the roadway increases sharply within 50 m from the heading face. Compared with the normal area, the range of the stress surge stage and the vertical stress value increase by 43% and 63%, respectively. The fracture range of the roadway surrounding rock increases from 3 m to 5 m, and the fractures and separation layers increase. It is more difficult to control roadway deformation.

4. Support Optimization of Gob-Side Entry under the Influence of Fault

4.1. Support Optimization Concept

- (1) Optimize according to roadway deformation. After the influence of the fault, the stress of the roadway is partially concentrated. According to the above monitoring, the roadway in the fault area shows the deformation characteristics of a significant increase in the roof and floor and a significant side bulge. The roadway has a large degree of deformation and a fast deformation speed. Therefore, controlling large deformation and ensuring the relative integrity of the roadway are the main support goals. As an important support parameter, the pre-tightening force can effectively reduce the initial deformation of the roadway and maintain the integrity of the roadway to a large extent. At the same time, the single hydraulic prop and other passive supports can also effectively control the deformation of the top and bottom plates. In the aspect of restraining the deformation of the fault area along the goaf roadway, the control method combining the single prop and increasing the pre-tightening force of the bolt can be adopted [14].

TABLE 3: Breaking characteristics of cable in the fault area.

Failure form	Failure characteristics	Picture of actual failure on-site
The central steel strand is broken first	The central steel strand of the exposed end cable is "protruding," and the cable is broken by several times	
Final breaking of central steel strand	The central steel strand of the exposed end cable is in the form of "core pulling," and the cable is broken several times	

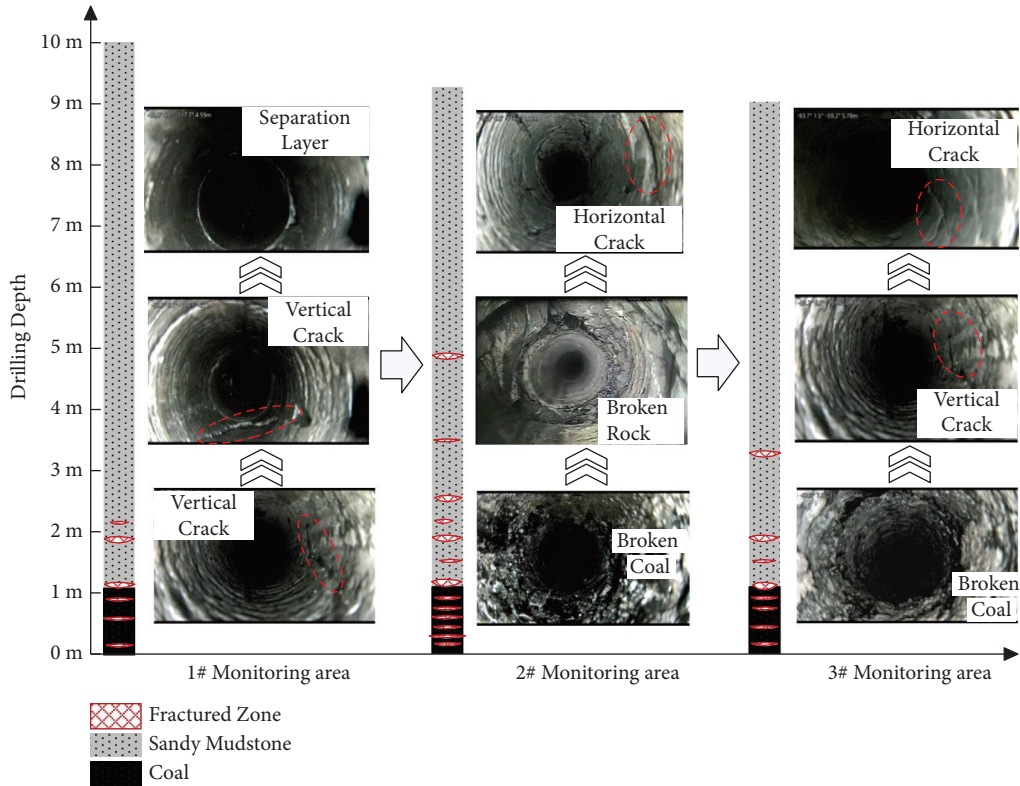


FIGURE 4: Results of the borehole TV survey.

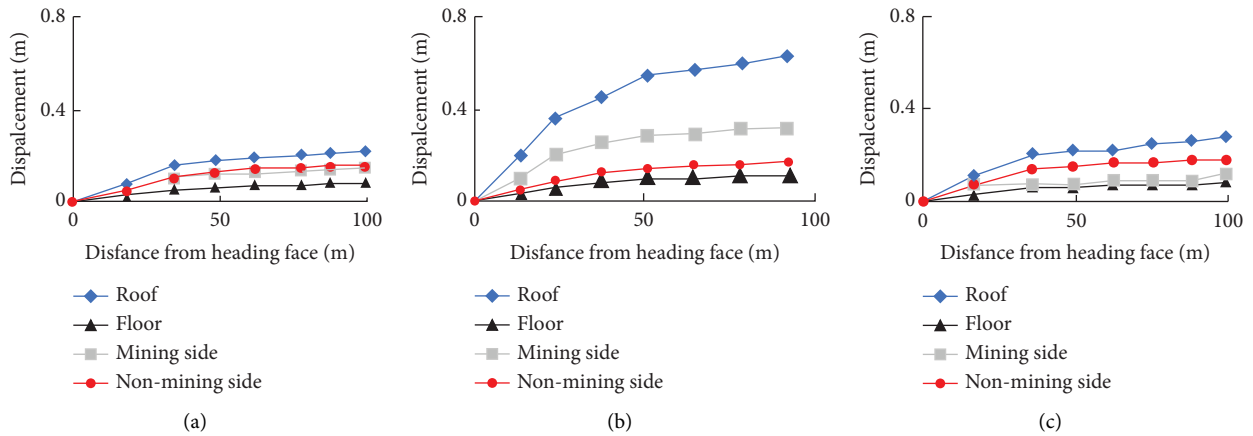


FIGURE 5: Monitoring results of roadway surface displacement. (a) 1# survey area. (b) 2# survey area. (c) 3# survey area.

(2) Optimize according to the stress evolution. The stress increase of gob-side roadway in fault area is high and fast due to mining. While ensuring the integrity of the roadway, it is also necessary to prevent accidents such as rock bursts caused by the stress accumulation of the roadway. Therefore, pressure relief measures should be taken at the advanced working face. Large-diameter pressure relief holes are relatively simple to implement and have a good application effect and are widely used in roadway pressure relief. Therefore, because of the stress evolution characteristics of a gob-side roadway in a fault area, the stress concentration

can be effectively improved by drilling large diameter relief holes at the advanced working face.

4.2. Support Optimization Simulation Study. The implementation parameters of a single prop are relatively simple, and they need to be determined in coordination with field equipment. In view of the roadway under this condition, the prop support scheme adopted is as follows: a row of single-props is set every 1 m, three single-props were set in each row, and a top beam shall be added above the props. However, the determination of cable pre-tightening force parameters is

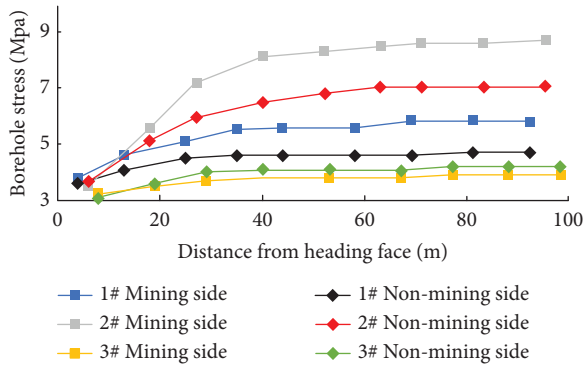


FIGURE 6: Surface displacement monitoring results.

relatively complex, and numerical simulation can better simulate and monitor the stress, deformation, and other characteristics of the roadway under different pre-tightening forces [15]. Therefore, this paper adopts a numerical simulation scheme to optimize the pre-tightening force.

4.2.1. Numerical Calculation Model and Scheme.

According to the geological conditions of coal and rock of 11302 tail entry, a numerical simulation model is established by using FLAC3D numerical simulation software. The model size is $58\text{ m} \times 30\text{ m} \times 30\text{ m}$, and the height and width of the roadway are 5.4 m and 3.6 m, while fixing the bottom boundary in the vertical direction, fixing the left and right boundaries and front and rear boundaries in the horizontal direction, and applying uniform stress on the top boundary in the vertical direction. The numerical simulation model is shown in Figure 7, and the mechanical parameters of coal and rock strata are shown in Table 4.

The supporting effects of the surrounding rock of the tunnel under three different supporting schemes, namely, no bolt (cable) support, low bolt-cable pre-tightening support, and high bolt-cable pre-tightening support coordination, are simulated, respectively. The respective supporting effects are compared and analyzed from the aspect of surrounding rock deformation, and the supporting scheme suitable for weakly cemented soft rock roadway is selected. The simulation scheme is shown in Table 5. Both the roof and the side are used $\Phi 22\text{ mm} \times 2400\text{ mm}$ bolt. The row spacing of bolts are $800\text{ mm} \times 800\text{ mm}$. The size of the roadway roof cable is $\Phi 21.8 \times 7300\text{ mm}$, and row spacing is $1600\text{ mm} \times 1600\text{ mm}$.

4.2.2. Analysis of Simulation Results. The cloud diagram of displacement distribution along the channel is shown in Figures 8 and 9, and the displacement change curve is shown in Figure 10. From the displacement distribution program, it can be seen that the vertical displacement is mainly concentrated on the roof, which is shown as the roof subsidence, and the horizontal displacement is mainly concentrated on the two sides, which is shown as the inner extrusion of the side. In Scheme 1, the maximum roof subsidence is 398 mm, and the displacement of two sides is 198 mm. In Scheme 2, the maximum subsidence of the roof is 296 mm, and the displacement of two sides is 116 mm. In Scheme 3, the

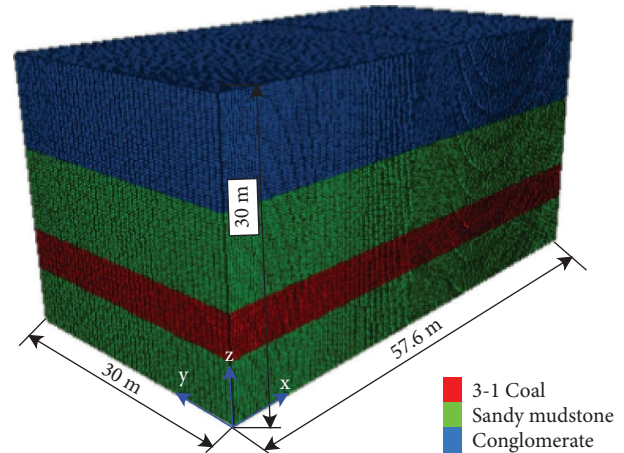


FIGURE 7: Numerical model and mesh generation.

maximum subsidence of roof is 79 mm, and the displacement of two sides is 55 mm. In Scheme 4, the maximum roof subsidence is 62 mm, and the displacement of two sides is 48 mm.

When Scheme 3 is adopted for support, the maximum subsidence of the roof decreases by 217 mm and 319 mm, respectively, compared with Scheme 2 and Scheme 1, and the displacement of two sides decreases by 61 mm and 143 mm, respectively, compared with Scheme 2 and Scheme 1. When Scheme 4 is adopted for support, the maximum subsidence of roof is reduced by 17 mm, 237 mm, and 336 mm, respectively, compared with Scheme 3, Scheme 2, and Scheme 1, and the displacement of two sides is reduced by 7 mm, 68 mm, and 150 mm, respectively, compared with Scheme 3, Scheme 2, and Scheme 1.

The above four support schemes show that different bolt cable support schemes have a great impact on the deformation of surrounding rock along the tunnel and have different effects on the deformation control of surrounding rock. The bolt cable high pre-tightening support coordination has the best control effect on the deformation of surrounding rock along the tunnel, and the deformation of surrounding rock is the smallest.

4.3. Field Application Effect. Eight working faces are arranged in the 3-1 coal seam of Hongqingliang Coal Mine in the west. The return air gateway of the 11303 working face is used as the gob-side roadway. There is a large fault near the main roadway. The above optimization measures for support are applied. The specific support and reinforcement measures are as follows: increase the pre-tightening force of the bolt to 70 kN, increase the pre-tightening force of the cable to 180 kN, increase the single hydraulic prop in the fault area, with the spacing of single pillars of 1 m, each row of single pillars is 3 for passive support, pressure relief holes with a diameter of 110 mm shall be drilled at the upper part, and the spacing between pressure relief holes shall be 1 m.

As shown in Figure 11, the deformation of the surrounding rock tends to be stable when it is about 120 m away from the heading face, the roof subsidence is about 42 mm,

TABLE 4: Mechanical parameters of coal and rock.

Rock stratum name	Density (kg/m ³)	Bulk modulus (GPa)	Shear modulus (GPa)	Internal friction angle (°)	Cohesion (MPa)	Tensile strength (MPa)
Conglomerate	2690	2.28	1.24	30	3.20	1.4
Sandy mudstone	2390	1.68	0.89	25	2.50	0.9
3-1 coal	1190	1.65	0.88	28	2.56	1.1

TABLE 5: Parameter table of weakly cemented soft rock roadway simulation scheme.

Bolt-cable support scheme	Different schemes	Bolt pre-tightening force (kN)	Cable pre-tightening force (kN)
No bolt-cable support	Scheme 1	0	0
Low pre-tightening support	Scheme 2	20	140
High pre-tightening support	Scheme 3	70	220

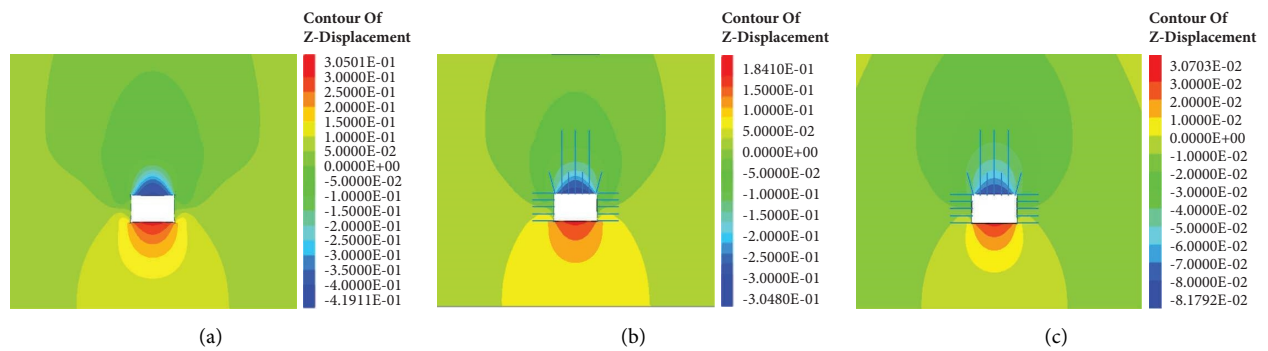


FIGURE 8: Cloud chart of vertical displacement distribution. (a) Scheme 1. (b) Scheme 2. (c) Scheme 3.

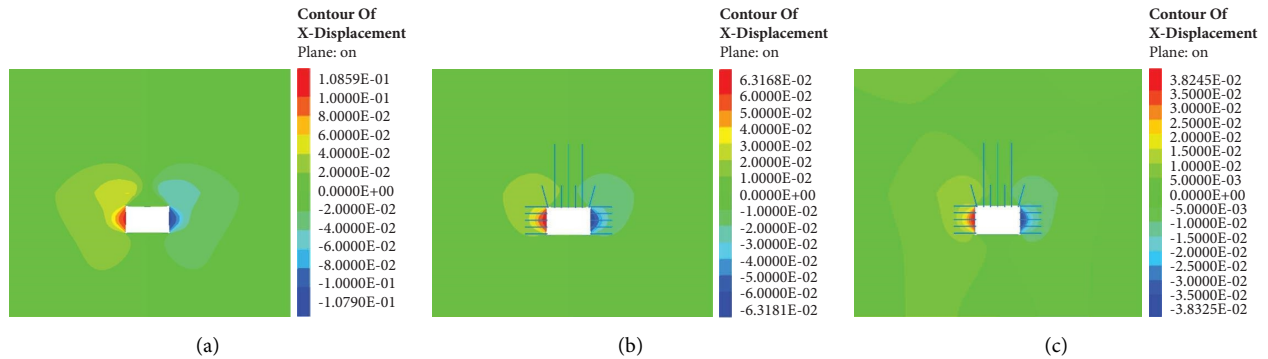


FIGURE 9: Cloud chart of horizontal displacement distribution. (a) Scheme 1. (b) Scheme 2. (c) Scheme 3.

and the movement of the two sides is 18 mm. The survey station shows that the deformation and stability time of the surrounding rock is shortened after the tunnel heading, the roof subsidence and the movement of two sides are not large, both within the controllable range, and the stability of the surrounding rock is good.

5. Discussion

The weakly cemented soft rock roadway is prone to significant damage under normal conditions due to the defects of its surrounding rock properties. When the roadway is in the fault-affected area, roadway deformation and damage are more obvious. In this paper, by studying the deformation

characteristics and stress evolution law of roadway in fault area, the optimization measures of weakly cemented soft rock roadway support in fault area are proposed and field experiments are carried out.

At present, weakly cemented soft rock roadway is prone to large-scale failure of the bolt, cable, and other support bodies in the fault area, and the failure characteristics are relatively consistent: the free section near the roof is broken and shows obvious multiple breaking characteristics. Therefore, how to better play the active support effect of bolt and cable on the roadway has become a key research object. Experts and scholars have put forward many theories and formed a wide range of support countermeasures against the failure of support bodies and the large deformation of

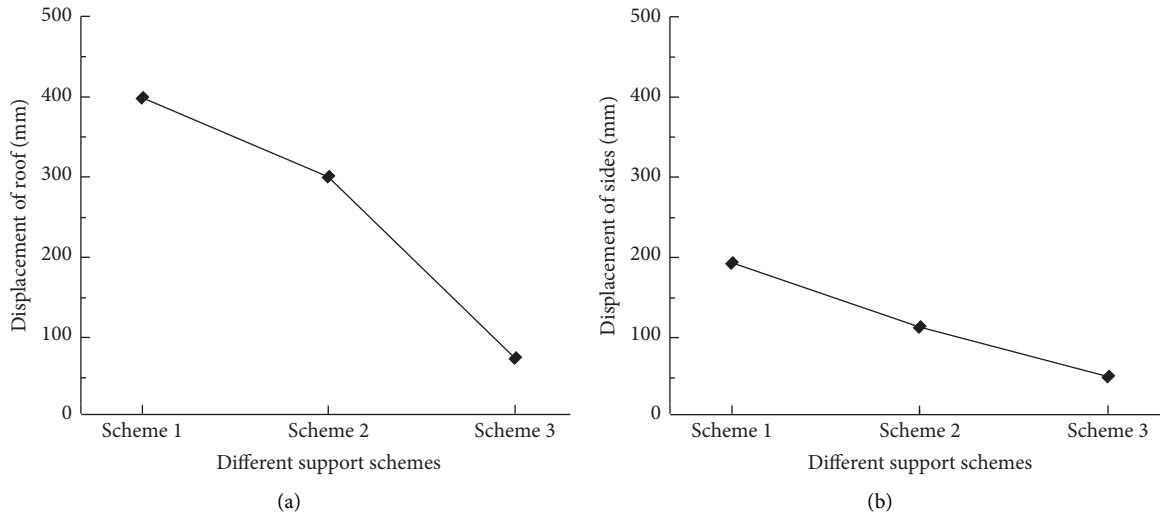


FIGURE 10: Displacement curve of surrounding rock surface. (a) Roof-floor. (b) Sides.

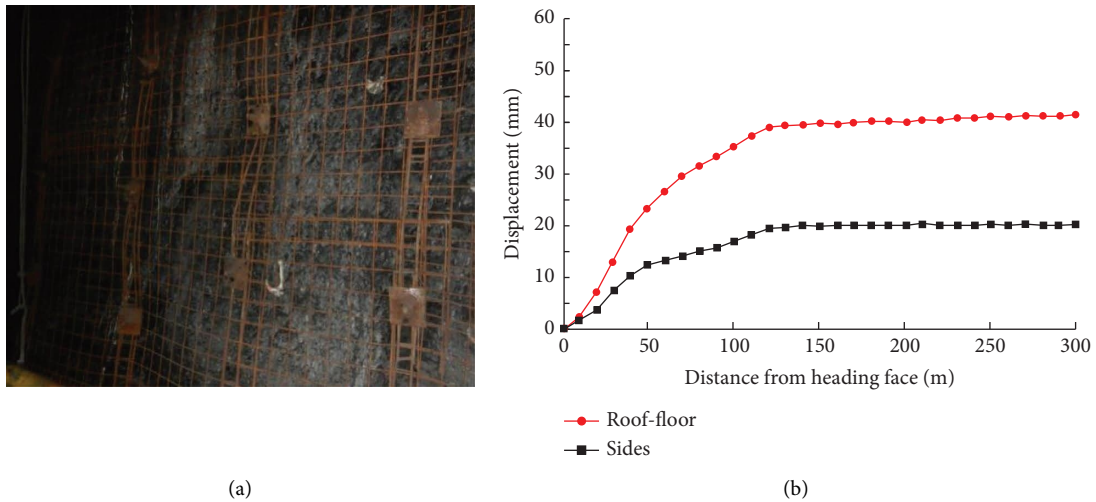


FIGURE 11: Roadway deformation after support optimization. (a) Actual effect of roadway. (b) Surface displacement characteristics.

roadways. For example, active support technologies such as constant resistance large deformation bolts [16, 17], bolt beam net support [18], and U-shaped steel support [19, 20] can effectively control the deformation of roadways.

However, for weakly cemented soft rock roadways, especially under the influence of fault, the research on roadway support technology needs to be enriched, and the above technology support costs are high. At present, bolt cable cooperative support is widely used in coal mine roadways, which is a basic support mode. In the above study, the failure characteristics of cables in fault areas were divided into two types: ① the central steel strand first broke and ② the surrounding steel strand first broke. How to optimize the bolt cable support characteristics to reduce the overall deformation of the roadway has become the focus of research [21]. The bolt-cable high pre-tightening support proposed in this paper can preliminarily reinforce the surrounding rock of the roadway and reduce the roadway deformation in the rapid deformation stage of the roadway after tunneling, thus

effectively ensuring the stability of the roadway and achieving good field application results.

6. Conclusions

In this paper, the following conclusions are obtained by studying the law of ground pressure behavior of weakly cemented soft rock roadway in fault areas and corresponding support optimization measures:

- (1) Affected by the mining stress of the previous working face, the gob-side roadway is seriously deformed after tunneling, and the ground pressure of the fault roadway is more intense, showing the characteristics of overall subsidence and poor formation of the roof, and the cable is broken in a large area by strands. The length of the broken cable is 0.2 m–0.6 m (regardless of the exposed end). The main failure characteristics of the cable are brittle fracture at the fracture of each steel strand, and the diameter shrinkage is not

obvious. The failure of cable in a fault area is characterized by dynamic load breaking.

- (2) The rock pressure monitoring results in the fault area obtained the stress evolution law of the roadway. The stress of the roadway in the fault-affected area increased significantly within the range of 50 m from the heading face. The affected area and the maximum vertical stress increased by 43% and 63%, respectively, compared with the normal area. The overall damage range of the roadway increased by 67%. The large degree of wall rock fracture in the free section of the cable led to a serious failure of the cable. Cable breakage exhibits the characteristic of “segmented breakage.”
- (3) According to the characteristics of roadway deformation and stress evolution, the support optimization strategy of restraining large deformation + pressure relief is proposed, the comprehensive support optimization scheme of bolt cable high preload + single prop + pressure relief is proposed, the optimal bolt cable preload is obtained through simulation, and specific support optimization measures are proposed. Field experiments show that the deformation and failure of roadway surrounding rock are effectively controlled.

Data Availability

The data used to support the findings of this study are available from the corresponding author.

Conflicts of Interest

The authors declare that they have no conflicts of interest.

Authors' Contributions

Chengfu Ma was responsible for the conception and writing tasks of the manuscript. Fenghai Yu was responsible for the data management and methodology of the manuscript. Kai Zhou was responsible for the numerical simulation and data analysis of the manuscript. Xuerui Yang was responsible for the on-site application of the manuscript. Bo Sun assisted in completing the original draft of the manuscript. Xinyu Yao assisted in completing the on-site measurement part of the manuscript. Yani Chi assisted in completing the numerical simulation of the paper. Yuanzhi Zhang assisted in completing data management of the manuscript.

Acknowledgments

This study was supported by the General Program of the Shandong Natural Science Foundation (ZR2022ME158).

References

- [1] K. Zhou, F. H. Yu, Y. L. Tan, T. Zhao, and W. Guo, “In-situ investigation on fractured evolution law of surrounding rock in weakly cemented soft rock roadway,” *Energy Sources, Part A: Recovery, Utilization, and Environmental Effects*, vol. 2021, pp. 1–13, 2021.
- [2] O. Vardar, C. C. Wei, C. G. Zhang, and I. Canbulat, “Numerical investigation of impacts of geological faults on coal burst proneness during roadway excavation,” *Bulletin of Engineering Geology and the Environment*, vol. 81, no. 1, pp. 2–21, 2022.
- [3] Q. Wang, Y. Wang, M. C. He et al., “Experimental study on the mechanism of pressure releasing control in deep coal mine roadways located in faulted zone,” *Geomechanics and Geophysics for Geo-Energy and Geo-Resources*, vol. 8, no. 2, p. 50, 2022.
- [4] R. L. Shan, Z. L. Li, C. H. Wang et al., “Research on the mechanism of asymmetric deformation and stability control of near-fault roadway under the influence of mining,” *Engineering Failure Analysis*, vol. 127, Article ID 105492, 2021.
- [5] S. Yan, J. B. Bai, W. F. Li, J. G. Chen, and L. Li, “Deformation mechanism and stability control of roadway along a fault subjected to mining,” *International Journal of Mining Science and Technology*, vol. 22, no. 4, pp. 559–565, 2012.
- [6] X. W. Liu, J. X. Chen, B. Liu, Y. Luo, Y. G. Zhu, and X. Huang, “Large deformation disaster mechanism and control technique for deep roadway in faulted zone,” *Frontiers in Earth Science*, vol. 10, Article ID 826661, 2022.
- [7] X. G. Sun, H. B. Wang, X. F. Wo, Z. M. Sun, W. L. Sun, and C. Li, “Roadway deformation and control under multi-disturbed secondary high stress,” *Geofluids*, vol. 2022, 12 pages, Article ID 3166065, 2022.
- [8] Z. Q. Ma, X. C. Liang, Y. Liu, G. Y. Wu, Y. D. Jiang, and Y. Q. Cao, “Real-time detection and information-based construction of roadways passing through faults: a case study,” *Environmental Earth Sciences*, vol. 80, no. 9, p. 339, 2021.
- [9] H. W. Wang, Y. D. Jiang, S. Xue et al., “Assessment of excavation damaged zone around roadways under dynamic pressure induced by an active mining process,” *International Journal of Rock Mechanics and Mining Sciences*, vol. 77, pp. 265–277, 2015.
- [10] S. R. Xie, Y. Y. Wu, D. D. Chen, R. P. Liu, X. T. Han, and Q. C. Ye, “Failure analysis and control technology of intersections of large-scale variable cross-section roadways in deep soft rock,” *International Journal of Coal Science & Technology*, vol. 9, no. 1, p. 19, 2022.
- [11] X. J. Yang, J. W. Pang, D. M. Liu et al., “Deformation mechanism of roadways in deep soft rock at Hegang Xing’an Coal Mine,” *International Journal of Mining Science and Technology*, vol. 23, no. 2, pp. 307–312, 2013.
- [12] X. Chen and J. Wu, “Study on the mechanism and control technology of large deformation of roadway surrounding rock in the fault fracture zone,” *Journal of Mining and Safety Engineering*, vol. 35, no. 5, pp. 885–892, 2018.
- [13] Y. S. Yang, Z. M. Fang, G. Y. Ji, B. G. Zhao, and S. J. Wei, “Study on mechanical properties and control technology of surrounding rock in the fracture zone of a roadway,” *Shock and Vibration*, vol. 2021, 14 pages, Article ID 6628593, 2021.
- [14] S. L. Wu, Y. C. Li, Y. Q. Chen, and L. Li, “Analysis and evaluation of support performance of multi-service support in Gaotouyao coal mine,” *Journal of Shandong University of Science and Technology*, vol. 39, no. 3, pp. 50–58, 2020.
- [15] Z. Wang, Y. C. Yin, T. B. Zhao, J. M. Ma, and W. B. Wu, “Numerical simulation study on bolting mechanism and support control of soft rock roadway,” *Journal of Shandong University of Science and Technology*, vol. 40, no. 3, pp. 35–43.
- [16] B. Wang, M. C. He, and Y. F. Qiao, “Resistance behavior of Constant-Resistance-Large-Deformation bolt considering surrounding rock pressure,” *International Journal of Rock*

- Mechanics and Mining Sciences*, vol. 137, Article ID 104511, 2021.
- [17] X. M. Sun, L. Cui, Y. Zhang, L. Wang, and Z. M. Qi, “Mechanical properties of rock with pre-cracks anchored by constant resistance and large deformation cables based on particle flow codes,” *Engineering Failure Analysis*, vol. 142, Article ID 106781, 2022.
- [18] G. Li, F. S. Ma, J. Guo, H. J. Zhao, and G. Liu, “Study on deformation failure mechanism and support technology of deep soft rock roadway,” *Engineering Geology*, vol. 264, Article ID 105262, 2020.
- [19] T. Li, R. L. Shan, H. S. Han, W. H. Yang, and N. Liu, “Mechanical mechanism and support design analysis on bolt-beam-net support in soft rock roadway in Qigou Coal Mine,” *Journal of Coal Science and Engineering*, vol. 18, no. 3, pp. 247–253, 2012.
- [20] K. Wang, L. G. Wang, and B. Ren, “Failure mechanism analysis and support technology for roadway tunnel in fault fracture zone: a case study,” *Energies*, vol. 14, no. 13, p. 3767, 2021.
- [21] G. F. Li, J. H. Wang, J. R. Liu et al., “Study on shear properties and failure characteristics of bolted joint of roadway surrounding rock,” *Journal of Shandong University of Science and Technology*, vol. 41, no. 4, pp. 47–55, 2022.